JOURNAL OF MAGNETIC RESONANCE, Series A 109, 14–25 (1994)

Distance Measurements between Homonuclear Spins in Rotating Solids

O. WEINTRAUB,* S. VEGA,* CH. HOELGER,† AND H. H. LIMBACH†

*Chemical Physics Department, The Weizmann Institute of Science, 76100 Rehovot, Israel; and †Institut für Organische Chemie, Freie Universität Berlin, D-14195 Berlin, Federal Republic of Germany

Received June 11, 1993; revised October 28, 1993

The effective Hamiltonian of the "simple excitation for the dephasing of the rotational-echo amplitudes" (SEDRA) experiment has been derived. This experiment enables the determination of the strength of the dipolar interaction of a homonuclear spin pair in a solid, rotating at the magic angle, and thus provides a way to measure internuclear distances. The dipolar decay of the rotational-echo amplitudes of powder samples, generated by a set of π pulses, is measured together with the echo decay that is not influenced by the dipolar interaction. The latter is measured by the transverse-echo SEDRA experiment that refocuses the SEDRA decay. The Floquet theory approach is utilized to evaluate the effective Hamiltonians that describe the behavior of the spin systems. The influence of the chemical-shift anisotropy parameters of the interacting spins on the effective SEDRA Hamiltonian is also discussed. Results of $\Delta S/S_0$ SEDRA experiments on the ^{15}N spin pair in solid 3(5)-methyl-5(3)-phenylpyrazole–$^{15}N_2$ are shown and compared with exact calculations. The data suggest a nuclear distance between the nitrogen atoms of 1.385 ± 0.025 Å.

INTRODUCTION

The dipolar interaction between nuclei is one of the most important interactions that influence the spectra in solid-state NMR. This interaction depends on the distance between the coupled nuclei. Measurements of its strength can therefore provide internuclear distances. In single crystals, spectral splitting enables the deduction of the dipolar interaction strengths. However, in powders, NMR spectra are usually characterized by broad and sometimes overlapping lineshapes. In order to increase the resolution and the sensitivity of the observed spectra, it is desirable to perform solid-state NMR experiments on samples rotating at the magic angle. This leads to partial or complete averaging of all anisotropic interactions that are defined by second-order tensors, such as the chemical shift, dipolar, and first-order quadrupolar interactions. Radiofrequency pulse schemes were designed to interfere with this averaging process, thereby reintroducing a selected interaction into the spectral behavior of spins.

In this publication, we will discuss the pulse sequence that consists of a simple excitation for dephasing of rotational-echo amplitudes (SEDRA) (*1–4*). This pulse method belongs to a set of experiments that were suggested to enhance significantly the influence of the homonuclear dipolar interaction on NMR signals of a rotating solid. Among these is the well-known rotational-resonance (R^2) experiment for homonuclear spin pairs (*5–15*). In this experiment one sets the spinning speed to satisfy the condition $\Delta_{12} = N\omega_R$, where ω_R is the spinning frequency, Δ_{12} is the isotropic chemical-shift difference, and N is any integer. Under this condition, the sidebands and centerband in the MAS spectra of spin pairs are broadened to an extent depending on the dipolar interaction. The analysis of the lineshapes of these bands can provide us with the dipolar interaction strengths. Another experimental approach is to monitor the exchange of magnetization between the coupled spins by measuring the decay of the difference between these magnetizations. This approach is applicable in particular for the detection of weak dipolar interactions (*6–8*). The R^2 experiments are highly selective in the sense that the resonance condition can be set independently for each type of coupled spin pairs in the sample that exhibits a discrete isotropic chemical-shift difference.

A different method for observing homonuclear interactions is to use pulse sequences that partially defeat the averaging process of MAS spectroscopy. Tycko *et al.* (*16*) proposed the DRAMA sequence for this purpose. This experiment consists basically of the application of two $\pi/2$ pulses during each rotor cycle period T_R. This causes only partial dipolar refocusing at the end of the rotor period and hence a dipolar-induced decay of the MAS powder signal. This scheme yields its best results when the two interacting nuclei have similar isotropic chemical-shift values. Chemical-shift anisotropy parameters and isotropic shift differences, although partially compensated by π pulses, influence the DRAMA decays and should be taken into account during data analysis. Extensions of this approach toward double-quantum filtering techniques lead to selective spectral excitations (*17*).

Gullion *et al.* introduced the rotational-echo double-resonance (REDOR) technique for the detection of dipolar interactions between heteronuclear spins (*18–20*). An extension of this experiment was introduced by Hing *et al.* in the form of their transfer-echo double-resonance (TEDOR) scheme (*21*). In these MAS experiments, a pair of π pulses

1064-1858/94 $6.00

are applied to each rotor cycle and the signal is acquired at the end of each rotor cycle or after a set of rotor periods. Another interesting experiment for deducing dipolar interaction strengths in solids is the zero-field–high-field method, also proposed by Tycko (*22, 23*). Here both RF pulses and sample rotations off the magic angle are used to transform the orientation-dependent truncated Hamiltonian into a scalar (orientation-independent) Hamiltonian.

The SEDRA experiment for homonuclear dipolar dephasing also relies on synchronously applied RF pulses (*1, 3, 4, 18*). The basic time unit for this experiment is $2T_R$ and one single π pulse is applied during each rotor cycle. This method refocuses the decays due to chemical-shift anisotropy (CSA) interactions of uncoupled spins, but induces signal dephasing due to the dipolar interaction between coupled spins.

In this publication, we derive the effective Hamiltonian governing the SEDRA experiment, using the Floquet formalism. This formalism was proven to be very convenient and informative for the description of MAS experiments. Various examples of its use were discussed earlier (*9, 11, 24, 25*). An average Hamiltonian for the basic SEDRA pulse sequence in the RF driven dipolar recoupling (RFDR) experiment has already been derived by Bennet *et al.* (*3*). A vector model representation of this experiment was suggested by Sodickson *et al.* (*4*).

In the next section, the effective SEDRA Hamiltonian of a homonuclear-coupled spin pair will be derived, taking into account the influence of the chemical-shift anisotropies of the spins. Then the transverse-echo SEDRA experiment will be introduced and its effective Hamiltonian derived. This experiment will measure the contributions to signal decays that are not caused by the SEDRA sequence and, when combined with SEDRA, will provide an accurate determination of the dipolar interaction and hence an intramolecular distance. In the last section, experimental results, obtained from SEDRA experiments on a fully ^{15}N-enriched powder sample of 3(5)-methyl-5(3)-phenylpyrazole, will be shown.

THE SEDRA EXPERIMENT

In this section, the theory of the SEDRA experiment is discussed in terms of the Floquet theory in order to show the full derivation of the effective SEDRA Hamiltonian as presented before (*1, 3, 4*). At first, the time-dependent Hamiltonian of a dipolar-coupled homonuclear spin pair, rotating at the magic angle, is used to construct a time-independent Floquet Hamiltonian. The steps required to convert a periodically time-dependent Hamiltonian into a time-independent Floquet Hamiltonian were described elsewhere (*26*). This Floquet Hamiltonian is represented in the toggling frame, defined by the RF irradiation part of the original Hamiltonian, and then expressed in terms of the Floquet operators and exploited to derive an effective SEDRA Hamiltonian. This Hamiltonian should describe the stroboscopically detected signal decay. For our theoretical derivations we assume infinitely short π pulses.

THE EFFECTIVE SEDRA HAMILTONIAN

The pulse sequence for the SEDRA experiment on a homonuclear spin pair is shown in Fig. 1a. The basic unit of the SEDRA experiment for infinitely short π pulses consists of two rotor periods $2T_R$ with two π pulses inserted at positions $1/2T_R$ and $3/2T_R$. In order to follow the effect of this pulse scheme on the spin system, we first write the spin Hamiltonian of the spin pair without its RF part,

$$\begin{aligned}\mathcal{H}(t) = &-\omega_1^{cs}(t)I_{z1} - \omega_2^{cs}(t)I_{z2} + 2\omega_D(t)\\ &\times \{I_{z1}I_{z2} - \tfrac{1}{4}(I_1^+I_2^- + I_1^-I_2^+)\}\\ &+ J\{I_{z1}I_{z2} + \tfrac{1}{2}(I_1^+I_2^- + I_1^-I_2^+)\}, \qquad [1]\end{aligned}$$

where $\omega_1^{cs}(t)$ and $\omega_2^{cs}(t)$ are the time-dependent CSA coef-

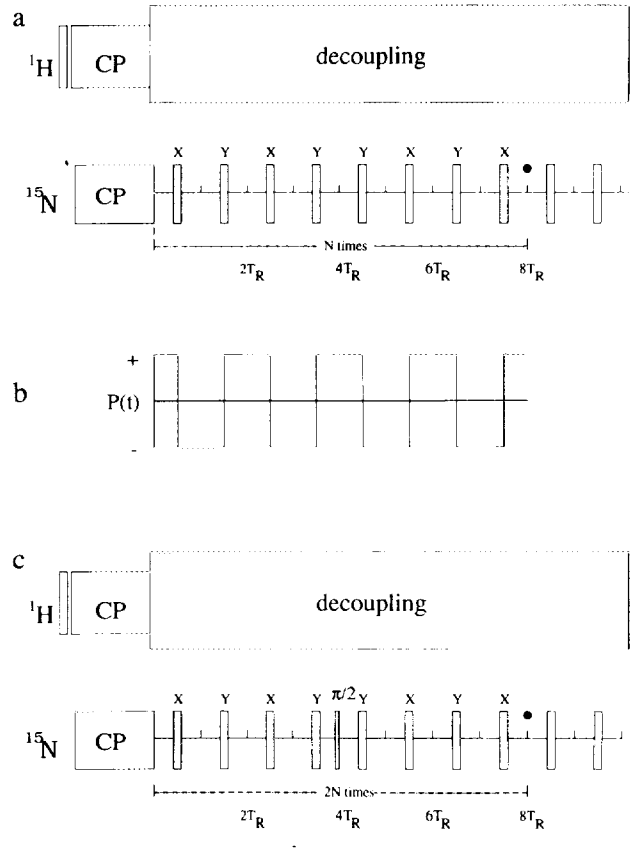

FIG. 1. In (a) the pulse scheme for the SEDRA experiment is shown. It consists of a cross-polarization period followed by a sequence of eight π pulses (four basic SEDRA cycles) with phases according to the XY-8 phase cycle. At the end of an integer set of cycles, signals are recorded. In (b) the time-dependent function $p(t)$ is given. This function modulates only the chemical-shift part of the Hamiltonian, causing the average of the off resonances to vanish for all spinning speeds. In (c) the transverse-echo SEDRA (t-SEDRA) is shown. It reassembles the SEDRA sequence with the addition of one $\pi/2$ pulse to refocus dephasing due to the dipolar interaction.

ficients of spin-1 and spin-2, respectively, $\omega_D(t)$ is the dipolar interaction coefficient, and J is the indirect scalar coupling. The explicit forms of those coefficients are given elsewhere (*27, 26*) and are repeated for convenience in Appendix A. The off-resonance values and the isotropic chemical-shift values $\Delta\omega_1$ and $\Delta\omega_2$ of the spins are contained in $\omega_1^{cs}(t)$ and $\omega_2^{cs}(t)$, respectively.

In the manifold of spin states $|1\rangle = |\alpha_1\alpha_2\rangle$, $|2\rangle = |\alpha_1\beta_2\rangle$, $|3\rangle = |\beta_1\alpha_2\rangle$, and $|4\rangle = |\beta_1\beta_2\rangle$, this Hamiltonian can be written, using the fictitious spin-$\frac{1}{2}$ operators, as

$$\mathcal{H}(t) = -\{\omega_1^{cs}(t) + \omega_2^{cs}(t)\}I_z^{14} - \{\omega_1^{cs}(t) - \omega_2^{cs}(t)\}I_z^{23} + \left\{\omega_D(t) + \frac{J}{2}\right\}(I_z^{12} - I_z^{34}) - \{\omega_D(t) - J\}I_x^{23}. \quad [2]$$

In order to involve the π pulses, we transform this Hamiltonian to the RF toggling frame. This introduces an additional time dependence into the Hamiltonian which can be written as

$$\mathcal{H}(t)^T = -\{\omega_1^{cs}(t) + \omega_2^{cs}(t)\}p(t)I_z^{14} - \{\omega_1^{cs}(t) - \omega_2^{cs}(t)\}p(t)I_z^{23} + \left\{\omega_D(t) + \frac{J}{2}\right\} \times (I_z^{12} - I_z^{34}) - \{\omega_D(t) - J\}I_x^{23}. \quad [3]$$

The dipolar and the J-coupling part of the Hamiltonian are left unchanged under the influence of the π pulses. The form of the time-dependent function $p(t)$ is given in Fig. 1b. When the time-dependent coefficients of the Hamiltonian are expanded in their Fourier series with a time period $2T_R$ and with $\omega_R = 2\pi/T_R$, we get

$$-[\omega_1^{cs}(t) + \omega_2^{cs}(t)] = 2\sum_{m=-2}^{2}(\omega_1^{cs} + \omega_2^{cs})_{2m}e^{i2m(\omega_R/2)t}$$

$$-[\omega_1^{cs}(t) - \omega_2^{cs}(t)] = 2\sum_{m=-2}^{2}(\omega_1^{cs} - \omega_2^{cs})_{2m}e^{i2m(\omega_R/2)t}$$

$$p(t) = \sum_{n=-\infty}^{\infty} p_n e^{in(\omega_R/2)t}$$

$$\omega_D(t) = 2\sum_{m=-2}^{2}\omega_{2m}^{D}e^{i2m(\omega_R/2)t}. \quad [4]$$

The coefficients $(\omega_1^{cs} \pm \omega_2^{cs})_{2m}$ and ω_{2m}^D for $m = \pm 1, \pm 2$ are the nonzero Fourier components of the chemical shift and the dipolar interaction, respectively, as given explicitly in Appendix A.

An important parameter is the off-resonance difference between the two spins $\Delta_{12} = 2(\omega_2^{cs} - \omega_1^{cs})_0 = \Delta\omega_2 - \Delta\omega_1$. The toggling-frame Hamiltonian of Eq. [3] can now be transformed into the time-independent Floquet Hamiltonian $\mathbf{H}_F$,

$$\mathbf{H}_F^T = \sum_{p=1}^{4}\frac{1}{2}\omega_R N^{pp} + \sum_{n=-\infty}^{\infty} 2\{\omega_n^{14}Z_n^{14} + \omega_n^{23}Z_n^{23}\} + \sum_{n=-\infty}^{\infty} 2\{\Omega_n^z(Z_n^{12} - Z_n^{34}) - \Omega_n^x X_n^{23}\}, \quad [5]$$

which can also be written using the single-block Z^{pp} operators:

$$\mathbf{H}_F^T = \sum_{p=1}^{4}\frac{1}{2}\omega_R N^{pp} + \sum_{p=1}^{4}\sum_{n=-\infty}^{\infty} 2\omega_n^{pp}Z_n^{pp} - \sum_{n=-\infty}^{\infty} 2\Omega_n^x X_n^{23}. \quad [6]$$

The various coefficients in $\mathbf{H}_F^T$ are defined as

$$\omega_n^{14} = \sum_{m=-2}^{2}(\omega_1^{cs} + \omega_2^{cs})_{2m}p_{n-2m}$$

$$\omega_n^{23} = \sum_{m=-2}^{2}(\omega_1^{cs} - \omega_2^{cs})_{2m}p_{n-2m}$$

$$\Omega_{2m}^z = \omega_{2m}^D, \qquad \Omega_0^z = \frac{J}{4}$$

$$\Omega_{2m}^x = \omega_{2m}^D, \qquad \Omega_0^x = -\frac{J}{2}$$

$$\omega_n^{11} = \omega_n^{14} + \Omega_n^z, \qquad \omega_n^{22} = \omega_n^{23} - \Omega_n^z$$

$$\omega_n^{33} = -\omega_n^{23} - \Omega_n^z, \qquad \omega_n^{44} = -\omega_n^{14} + \Omega_n^z. \quad [7]$$

In this Hamiltonian we use the Floquet operators which are defined as (*27*)

$$\langle pm + n|Z_n^{pp}|pm\rangle = \langle qm + n|Z_n^{qq}|qm\rangle = \frac{1}{2}$$

$$\langle pm + n|Z_n^{pq}|pm\rangle = -\langle qm + n|Z_n^{pq}|qm\rangle = \frac{1}{2}$$

$$\langle pm + n|X_n^{pq}|qm\rangle = \langle qm + n|X_n^{pq}|pm\rangle = \frac{1}{2}$$

$$\langle pm + n|Y_n^{pq}|qm\rangle = \langle qm + n|Y_n^{pq}|pm\rangle^* = -\frac{i}{2}. \quad [8]$$

The operators allow a convenient representation of the infinite Floquet matrices. The last term in $\mathbf{H}_F^T$ represents the flip-flop term in $\mathcal{H}(t)$. Its matrix elements are off-diagonal in the off-diagonal block $\{|2n\rangle, |3n\rangle\}$. For heteronuclear spin pairs, this term may be ignored. The block-diagonal part of the Hamiltonian of Eq. [5] can be diagonalized by the matrix $\mathbf{D}_F$ (*26, 27*),

$$\mathbf{D}_F = \sum_{p=1}^{4} \sum_{n=-\infty}^{\infty} \{2d_n^{pp} Z_n^{pp}\}, \quad [9]$$

where the coefficients d_n^{pp} can be calculated by the Fourier transform

$$\sum_{n=-\infty}^{\infty} d_n^{pp} e^{in\omega_R t} = \exp\left\{-\sum_{-\infty}^{\infty} \frac{\omega_n^{pp}}{n\omega_R}(e^{in\omega_R t} - 1)\right\}, \quad [10]$$

and where $2\omega_n^{pp}$ are the coefficients of the Z_n^{pp} operators in $\mathbf{H}_F^T$. The derivation of the equality in Eq. [10] is presented in Appendix B. In the special case that only the $\omega_{\pm 1}^{pp} = \omega_1^p e^{\pm i\phi_p}$ elements are different from zero, the solutions to the d_n^{pp} coefficients can be expressed in terms of Bessel functions (*29*) and become

$$d_n^{pp} = J_n(x)e^{in\phi_p}, \quad x = \frac{-2\omega_1^p}{\omega_R}. \quad [11]$$

The details of this approach are discussed in Appendix C.

Applying the diagonalization matrix to the Hamiltonian of Eq. [5] yields

$$\mathbf{D}_F^{-1}\mathbf{H}_F^T\mathbf{D}_F = \sum_{p=1}^{4} \frac{1}{2}\omega_R N^{pp} + 2\{\omega_0^{14} Z_0^{14} + \omega_0^{23} Z_0^{23} + \Omega_0^z(Z_0^{12} - Z_0^{34})\} - \sum_{n=-\infty}^{\infty} 2\Omega_n^x \mathbf{D}_F^{-1} X_n^{23} \mathbf{D}_F. \quad [12]$$

Since the Fourier expansion of $p(t)$ in Eq. [4] gives $p_{2m} = 0$ for $m = 0, \pm 1, \pm 2, \ldots$, the coefficients ω_0^{14} and ω_0^{23} are zero. Thus we get a Z-diagonalized toggling-frame Floquet Hamiltonian for the SEDRA experiment of the form

$$\mathbf{H}_F^T = \sum_{p=1}^{4} \frac{1}{2}\omega_R N^{pp} + 2\Omega_0^z(Z_0^{12} - Z_0^{34}) + \sum_{n=-\infty}^{\infty} \omega_n^{eff} \times (X_n^{23} + iY_n^{23}) + \omega_n^{eff*}(X_n^{23} - iY_n^{23}), \quad [13]$$

where

$$\omega_n^{eff} = -\sum_{k,m=-\infty}^{\infty} d_k^{22-1}\Omega_{m+n-k}^x d_{-m}^{33}. \quad [14]$$

This Hamiltonian can be utilized to evaluate the effective SEDRA Hamiltonian. As was shown elsewhere (*27*), the Z-diagonalized toggling-frame Floquet Hamiltonian represents the Floquet Hamiltonian of the spin system as long as the toggling-frame transformation is cyclic and the system is monitored synchronously with its time period.

To utilize the $\mathbf{H}_F$ of Eq. [13] as a precursor to the time-independent effective Hamiltonian, we assume that only the diagonal part of the nondiagonal $\{|2n\rangle, |3n\rangle\}$ block is significant. This assumption is justified when the dipolar strength is small compared to the spinning speed. The element ω_0^{eff} is complex in general; however, under the above conditions, it becomes real and hence the SEDRA Floquet Hamiltonian can be written as

$$\mathbf{H}_F^T = \sum_{p=1}^{4} \frac{1}{2}\omega_R N^{pp} + 2\{\omega_0^{eff} X_0^{23} + \Omega_0^z(Z_0^{12} - Z_0^{34})\}. \quad [15]$$

The effective Hamiltonian can now be constructed by transforming the Floquet Hamiltonian back to the normal spin-Hamiltonian form (*27*):

$$\bar{\mathscr{H}}^T = 2\left\{\omega_0^{eff} I_x^{23} + \frac{J}{4}(I_z^{12} - I_z^{34})\right\} = \omega_0^{eff}(I_1^+ I_2^- + I_1^- I_2^+) + J I_{z1} I_{z2}. \quad [16]$$

Hence the SEDRA effective Hamiltonian consists only of a flip-flop term multiplied by a scaled dipolar interaction factor and a diagonal term which corresponds to the indirect coupling.

In order to obtain an estimate for the value of ω_0^{eff}, we notice that the terms arising on the diagonal of the X block of $\mathbf{H}_F^T$ are given by

$$\omega_0^{eff} = -\sum_{k,m=-\infty}^{\infty} d_k^{22-1}\Omega_{m-k}^x d_{-m}^{33}. \quad [17]$$

The effective Hamiltonian can now be used to evaluate the signal measured after a set of m SEDRA cycles. If we are interested in monitoring the spin coherence after a cross-polarization excitation (*1*), the SEDRA signal becomes proportional to

$$S_{SEDRA}(2mT_R) = \langle I_x^1 + I_x^2\rangle(t) = \langle I_x^1 + I_x^2\rangle(0) \times \cos\left(\left[\omega_0^{eff} - \frac{J}{2}\right]2mT_R\right). \quad [18]$$

However, if we want to follow the exchange of magnetization between the spins in the RFDR experiment (*3, 4*), the system must be prepared into an initial state $(I_z^1 - I_z^2)$ and the magnetization difference must be detected:

$$S_{SEDRA}(2mT_R) = \langle I_z^1 - I_z^2\rangle(t) = \langle I_z^1 - I_z^2\rangle(0)\cos(2\omega_0^{eff} 2mT_R). \quad [19]$$

The above expressions for the SEDRA signal are orientationally dependent via the values of ω_0^{eff}. Hence, for the

analysis of powder signals, proper integration over Euler angles must be performed. The values of ω_0^{eff} for the different orientations can be calculated using Eq. [10] and inserting the various d_n coefficients into Eq. [17]. For small values of the CSA parameters and weak dipolar interactions, an approximate expression for ω_0^{eff} can be derived, using Bessel functions. The details of this approximation are discussed in Appendix C. In Fig. 2 the dependence of ω_0^{eff} on the isotropic chemical-shift difference of a spin pair in a single crystal is shown and compared with its approximated values.

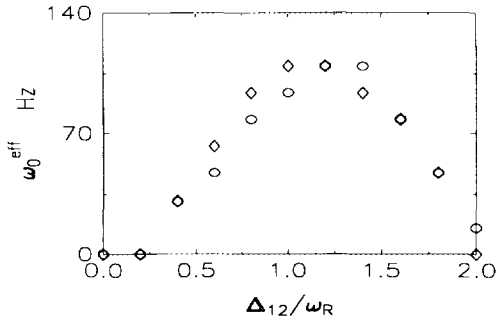

FIG. 2. Calculated values of the SEDRA effective frequency for a single crystal. ◇, ω_0^{eff} values obtained by taking into account the full Hamiltonian; ○, ω_0^{eff} values using the approximation of Appendix C. The dipolar parameters in the calculation were ω_D = 400 Hz, θ_D = 30°, and ϕ_D = 40°. The spinning speed was taken to be ω_R = 4000 Hz.

TRANSVERSE-ECHO SEDRA

As long as we assume infinitely short pulses for the SEDRA experiment, the signal can be monitored at times $2mT_R$. When pulses of finite length are considered, one must use an appropriate scheme to minimize pulse imperfections and errors in pulse intensities. For this purpose we adopted the XY-8 pulse scheme (*1*). Hence in all subsequent experiments the signal is collected at times $8mT_R$ for integer m. The decay of the SEDRA signal is dominated by the dephasing of the individual oscillating signals of the microcrystals in the powder sample. The signal decays are also due to T_2 processes. To enable a comparison of experimental results of the decaying SEDRA signal amplitudes with simulations, one should try to minimize the effect of these additional decay processes and subtract the signals from uncoupled spins. Thus it is desirable to measure a quantity $\Delta S/S_0$ (*18*), defined by

$$\frac{\Delta S}{S_0} = \frac{S_{\text{SEDRA}}(8mT_R) - S_0(8mT_R)}{S_0(8mT_R)}, \qquad [20]$$

where $S_{\text{SEDRA}}(8mT_R)$ is the SEDRA decay and $S_0(8mT_R)$ is the signal independent of the dipolar dephasing process. This ratio eliminates the part of the signal decay that is due to relaxation processes, but introduces to some extent a dependence on the uncoupled spin signals through their presence in the denominator in $\Delta S/S_0$. When the concentrations of the spin pairs in the sample are known, a correction considering this contribution can be made.

We suggest measuring $S_0(8mT_R)$ by the dipolar refocusing pulse scheme depicted in Fig. 1c. This pulse sequence has a basic time unit of $8T_R$ and is similar to the normal SEDRA sequence with the addition of a $\pi/2$ pulse at the fourth rotational-echo position. We name this pulse technique the transverse-echo SEDRA experiment (t-SEDRA). In order to calculate the effective Hamiltonian of t-SEDRA, one must extend the experimental scheme to make it cyclic (*30, 31*). This can be accomplished by adding a second t-SEDRA cycle with a $\pi/2$ pulse in the opposite direction. The resulting cyclic t-SEDRA extends over 16 rotor cycles. We can use average Hamiltonian theory in order to obtain the effective t-SEDRA Hamiltonian. This average Hamiltonian can be derived from the effective SEDRA Hamiltonian of Eq. [16] by transforming the SEDRA Hamiltonian to a toggling frame, defined by the two $\pi/2$ pulses.

The toggling-frame Hamiltonian of the t-SEDRA pulse sequence is divided into three time intervals. In the first interval up to $4T_R$, this Hamiltonian looks like

$$1 :\Longrightarrow \tilde{\mathscr{H}}^{(1)} = \omega_0^{\text{eff}}[2I_{x1}I_{x2} + I_{y1}I_{y2}] + JI_{z1}I_{z2}.$$

During the second period, from $4T_R$ to $12T_R$, it becomes

$$2 :\Longrightarrow \tilde{\mathscr{H}}^{(2)} = \omega_0^{\text{eff}}[2I_{x1}I_{x2} + I_{z1}I_{z2}] + JI_{y1}I_{y2}$$

due to the $\pi/2$ pulses in the x direction. Finally, in the third period after the second $\pi/2$ pulse with opposite phase, from $12T_R$ to $16T_R$, we again get the same Hamiltonian as that in the first period,

$$3 :\Longrightarrow \tilde{\mathscr{H}}^{(1)} = \omega_0^{\text{eff}}[2I_{x1}I_{x2} + I_{y1}I_{y2}] + JI_{z1}I_{z2}$$

Because these three parts of the Hamiltonian commute, the average t-SEDRA Hamiltonian is their weighted sum; hence

$$\bar{\mathbf{H}} = \frac{\omega_0^{\text{eff}}}{2}[2I_{x1}I_{x2} + 2\mathbf{I}_1 \cdot \mathbf{I}_2] + \frac{J}{4}[2\mathbf{I}_1 \cdot \mathbf{I}_2 - 2I_{x1}I_{x2}]. \qquad [21]$$

In fact, from a practical point of view, this Hamiltonian describes the signal also after each eight rotor periods. Hence we can retain $8T_R$ as our basic unit for the description of both SEDRA and t-SEDRA experiments. If the initial magnetization, right after cross polarization, points along the x direction, namely if the density matrix $\rho(0)$ is proportional to $[I_{x1} + I_{x2}]$, at the end of one t-SEDRA period, it will come back to $[I_{x1} + I_{x2}]$. This is a direct consequence of the fact that the above Hamiltonian commutes with the sum of the two x components. The I_{x1} and I_{x2} terms, however, do not refocus individually. For example, the I_{x1} term in the density matrix, omitting the effect of J coupling, oscillates with a term proportional to $\cos^2(\omega_0^{\text{eff}}8T_R)$, arising from the initial I_{x1} coefficient itself, and a term with $\sin^2(\omega_0^{\text{eff}}8T_R)$, coming from the initial I_{x2} coefficient.

TABLE 1
^{15}N Chemical-Shift and Dipolar Tensor Parameters of Solid Doubly ^{15}N-labeled PMP[a]

	$-^{15}N=$		$-^{15}NH-$
σ_{iso}[b]	236 (4784)		167 (3385)
σ_{11}[b]	409 (8290)		267 (5412)
σ_{22}[b]	257 (5210)		165 (3345)
σ_{33}[b]	39 (790)		69 (1399)
Euler angles of the ($-^{15}NH-$) CSA tensor[c]	$\alpha = 242°$	$\beta = 90°$	$\gamma = 90°$
Polar angles of the dipolar vector[c]	$\theta_D = 90°$		$\phi_D = 111°$

[a] All values are taken from Ref. (*34*). For a definition of parameters, see Ref. (*34*).

[b] Values in ppm refer to solid $^{15}NH_4Cl$. Values in parentheses are in hertz for a spectrometer of 4.7 T.

[c] Values are derived from Ref. (*34*) and are defined with respect to the ($-^{15}N=$) CSA tensor.

As long as the effective SEDRA Hamiltonian in Eq. [16] is valid, the t-SEDRA Hamiltonian refocuses all CSA effects, J interactions, and the dipolar interaction itself. When the CSA parameters become comparable or larger than the spinning speed, one must be careful interpreting the SEDRA experiments with the help of the effective SEDRA and t-SEDRA Hamiltonians. In the discussion below, we propose a modified version of t-SEDRA that can be implemented when the CSA parameters become comparable to the spinning speed. In general, the off-diagonal elements in the original Z-diagonalized toggling-frame Floquet Hamiltonian can become significant, leading to a complex ω_0^{eff}. Only exact numerical calculations can provide the theoretical SEDRA behavior of the signals. Numerical calculations are also required when incorporating the effect of finite pulse lengths for the SEDRA and t-SEDRA cycles.

EXPERIMENTAL

As a demonstration of the SEDRA approach for the detection of internuclear distances, a set of experiments was performed on solid 3(5)-methyl-5(3)-phenylpyrazole-$^{15}N_2$ (PMP). This compound was synthesized according to the literature (*32, 33*), starting from hydrazine sulfate labeled to 95% in both nitrogen positions (Chemotrade, Leipzig). Solid PMP contains directly bound ^{15}N spin pairs of the type $-^{15}NH-^{15}N=$, characterized by a nitrogen distance of 1.36 Å (*34*). The dipolar coupling tensor, the components of the chemical-shift tensors of the protonated ($-^{15}NH-$), and the nonprotonated ($-^{15}N=$) nitrogen atoms of PMP and the relative orientation of the different tensors have been determined (*35*) by powder lineshape analysis and are listed in Table 1. The CPMAS experiments were done on a homebuilt spectrometer operating at 20.27 MHz for ^{15}N nuclei. From the table it follows that for this spectrometer, the difference Δ_{12} between the isotropic chemical-shift values equals 1.4 kHz. This value is rather small with respect to the principal values of the CSA tensors. Thus significant overlap of the MAS sideband patterns of the two spins is observed. In Fig. 3 the CPMAS experimental spectra of PMP are shown. The nonprotonated nitrogen $=N-$ gives rise to a signal at 235 ppm, and the protonated nitrogen $-NH-$ to a signal at 167 ppm, referenced to the single line of solid $^{15}NH_4Cl$. The results in Fig. 3a were obtained with a spinning speed of 2777 Hz, which is far from the rotational resonance condition. The results in Fig. 3b were measured with a speed of 1400 Hz, satisfying this condition.

For the SEDRA experiments, each $\Delta S/S_0$ decay curve is made up of six experiments with increasing numbers of SEDRA periods. The ^{15}N FID signals were collected after the application of the SEDRA pulses and Fourier transformation. The length of the SEDRA sequence was incremented by $8T_R$, so that the signals were collected after up to 48 rotor periods. For each total length $n \times 8T_R$ the SEDRA signal $S_{SEDRA}(n8T_R)$ was recorded, by adding the intensities of all center- and sidebands in the Fourier frequency spectra. The transverse-echo SEDRA signals $S_0(n8T_R)$ were recorded in a similar way after a multiple of eight rotor periods. In all experiments, the XY-8 phase-cycling (*1*) scheme was used for the π pulses. Each data point was a sum of 24 signals, accumulated with a repetition time of 30–40 seconds. In all experiments, the π pulses on ^{15}N and the irradiation field for cross polarization on ^{1}H were about 50 kHz. The CP

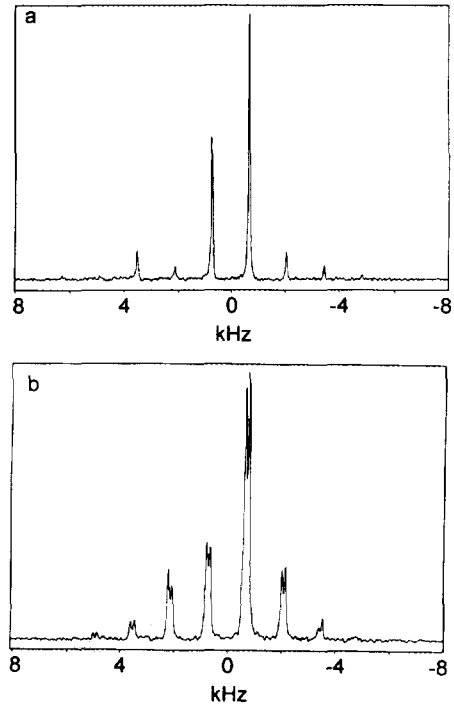

FIG. 3. CPMAS ^{15}N experimental spectra of the 3(5)-methyl-5(3)-phenylpyrazole molecule. In (a) the spinning speed is 2777 Hz, and in (b) a rotational-resonance ($N = 1$) spectrum is shown.

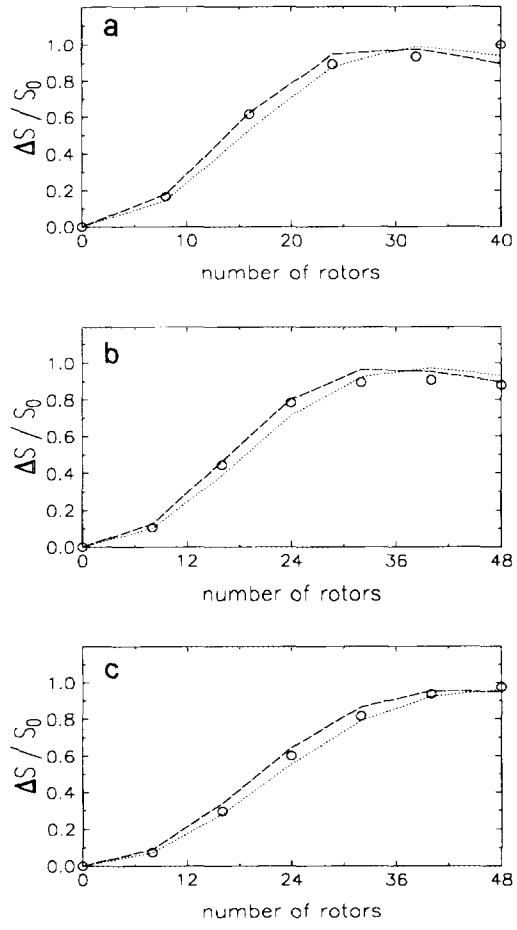

FIG. 4. The results of $\Delta S/S_0$ from SEDRA experiments on the ^{15}N nuclei in a fully ^{15}N-enriched sample of 3(5)-methyl-5(3)-phenylpyrazole. In these experiments, the spinning speeds were 2272 Hz in (a), 2500 Hz in (b), and 2777 Hz in (c). The experimental data are represented by circles in a proper size in order to include the experimental errors. Calculated results, including the effects of finite pulses, for a dipolar strength of 470 Hz are given by the upper dashed line and for a dipolar strength of 420 Hz by the lower dashed line. The parameters in Table 1 were used for these exact calculations.

mixing time was 4.5 ms. The proton decoupling power was about 100 kHz for the experiments at a spinning speed of 2777 Hz and about 65 kHz for all other spinning speeds. A rotor stabilizer was used and the spinning speed variations were smaller than ±10 Hz.

For the analysis of the data, a computer program was utilized that allows the evaluation of a large variety of NMR experiments on rotating spin pairs. In this program the density matrix of the spin system is calculated in all stages of the experiments. All CSA and dipolar parameters are taken into account. The program also allows incorporation of the lengths and the intensities of the pulses. The powder data are obtained by integration over all Euler angles using the method of Cheng *et al.* (*36*). In the actual calculations 550 sets of Euler angles were sufficient to generate the exact SEDRA decays.

RESULTS AND DISCUSSION

In Fig. 4 the results of the SEDRA experiments, performed at spinning speeds of 2272 Hz (Fig. 4a), 2500 Hz (Fig. 4b), and 2777 Hz (Fig. 4c), are shown. These spinning speeds are all larger than the difference between the isotropic chemical shifts of the interacting nuclei. As can be seen from Table 1, the CSA tensor elements are also larger than this difference. Thus it is apparent from the discussion above that the SEDRA decay will depend on these parameters and on the relative Euler angles of the tensors. Thus for the computer analysis it was essential to incorporate all the parameters of Table 1.

The circles in these figures represent the experimental $\Delta S/S_0$ results and their size represents the experimental errors. These results are compared with two simulated results for dipolar interaction strengths of 420 and 470 Hz. The computer simulations were performed by taking into account the lengths of the pulses as well as their phases. In all these calculations the XY-8 pulse scheme was used. It turned out that the length of the pulses can influence the calculated results significantly. Their influence is mainly noticeable when the spinning speed is much larger than the off-resonance difference. In order to demonstrate the difference between the values of $\Delta S/S_0$ for both finite and infinitely short

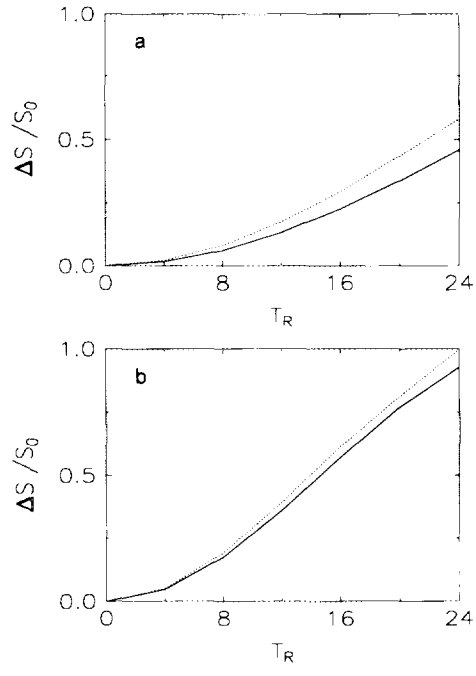

FIG. 5. The effect of the lengths of the π pulses is demonstrated by a simulation of $\Delta S/S_0$ of a powder sample with (a) $\Delta_{12}/\omega_R = 0.6$ and (b) $\Delta_{12}/\omega_R = 1.2$. In both cases the lower solid line corresponds to the results of SEDRA experiments with infinitely short pulses and the upper dashed line for π pulses with intensities of 50 kHz. The CSA and dipolar interaction parameters in the calculations were taken from Table 1. As can be seen, finite pulses enhance $\Delta S/S_0$ decay and must be taken into account during analysis, particularly when high spinning speeds are used.

pulses, two sets of simulated data for $\Delta_{12}/\omega_R = 0.6$ and for $\Delta_{12}/\omega_R = 1.2$ are shown in Figs. 5a and 5b, respectively. In both cases it can be seen that finite pulses lead to enhanced decays. When the spinning speed is substantially larger than the off-resonance difference Δ_{12}, a larger part of the observed signal decay may be due to pulse-length effects. Hence when working under such circumstances, one must be cautious not to misinterpret the experimental results. The incorporation of finite pulses and the effects of pulse imperfection on the SEDRA signal will be discussed more extensively elsewhere.

The data corresponding to $\Delta S/S_0$ values that are larger than 0.8 are not very reliable because at these values the individual SEDRA signals become very small. Figure 6 shows the results of the SEDRA experiments that were performed at a spinning speed of 3400 Hz. Again the data are compared with exact calculations for 470 and 420 Hz dipolar interactions, taking into account the parameters of Table 1, the length and the intensity of the pulses. This result deviates slightly from the values suggested in Fig. 4. The results given in Fig. 5 explain this behavior if we notice that at such a spinning speed, $\Delta_{12}/\omega_R = 0.4$, the efficiency of the SEDRA cycle is small, whereas other terms, like inaccurate pulse lengths or intensities mismatches, can become quite significant. In such circumstances, experimental instabilities can dominate the observed results. In Fig. 7, the experimental decays of the individual $S_{SEDRA}(8nT_R)$ and $S_0(8nT_R)$ are shown separately, in Fig. 7a for $\omega_R = 2777$ Hz and in Fig. 7b for $\omega_R = 3400$ Hz. The oscillation in the time dependence of $S_0(8nT_R)$ is also reproduced by the computer simulations.

Finally, from all the experimental results presented above, we can conclude that the dipolar interaction between the two nitrogens in PMP equals 445 ± 25 Hz. This range of values corresponds to a nuclear distance in the range of 1.385 ± 0.025 Å, which can be compared with X-ray (*35*) and neutron-diffraction (*37*) data on the same compound resulting in an internuclear distance of 1.36 or 1.345 Å deduced from NMR lineshape analysis of static powder spectra (*34*).

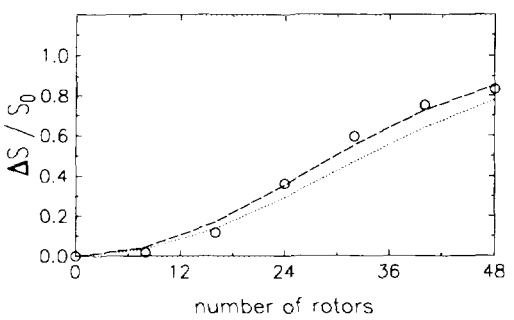

FIG. 6. The results of $\Delta S/S_0$ from SEDRA experiments on the ^{15}N nuclei in a fully ^{15}N-enriched sample of 3(5)-methyl-5(3)-phenylpyrazole. In these experiments the spinning speed was 3400 Hz. The experimental data are represented by circles of a proper size to include experimental error bars. Calculated results for a dipolar strength of 470 Hz are given by the upper dashed line and for a dipolar strength of 420 Hz by the lower dashed line. The parameters in Table 1 were used for these exact calculations. Here $\Delta_{12}/\omega_R = 0.42$. As evident from Fig. 5, at this regime the SEDRA scheme has only a minor effect on signal dephasing and other terms must be considered such as finite pulse length and pulse intensities mismatch. Indeed the results at this spinning speed seem to deviate slightly from the general trend illustrated by Fig. 4.

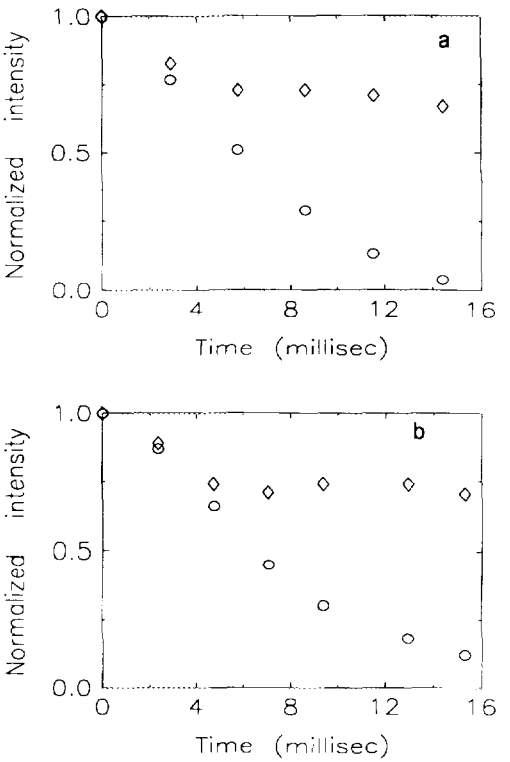

FIG. 7. Experimental results of $S_{SEDRA}(8nT_R)$ and $S_0(8nT_R)$ for the SEDRA experiments on 3(5)-methyl-5(3)-phenylpyrazole for a spinning speed of (a) 2777 Hz and (b) 3400 Hz. In both cases S_0 is marked by diamonds and S_{SEDRA} by circles.

CONCLUSIONS

We rederived the effective Hamiltonian for the SEDRA experiment using Floquet theory. We showed that the effective SEDRA frequencies can be approximated by a relatively simple expression in terms of the dipolar Fourier components and the elements of the eigenvectors of the SEDRA Floquet matrix. These elements can be obtained by a Fourier transformation of a function that contains the various CSA and dipolar parameters which appear in the Z blocks of this Hamiltonian. In order to partially eliminate the dephasing effects not due to the dipolar interaction, the t-SEDRA experiment was introduced. Finally, we have demonstrated the application of the SEDRA approach for determining homonuclear atomic distances on a doubly labeled ^{15}N PMP sample. For performing computer simulations it is desirable to know the CSA parameters and relative orientations in advance. The influences of these parameters on the experimental results manifest themselves mainly when the CSA

values become comparable to the off-resonance difference. In these cases, when tensorial angles are unknown, the computer analysis can only provide a bounded range of values for internuclear distances. As was pointed out, the influence of the length of the pulses of the SEDRA cycle must be taken into account during the analysis of the data. Thus accurate data analyses require the presence of a computer program that can handle the strength and duration of the pulses in the calculation. Of course, the influence of pulse lengths is not present when rotational-resonance experiments for homonuclear distance measurements are performed. The frequency selectivity of the rotational-resonance technique is also not present in the case of SEDRA; however, the facts that the frequency of rotation can be chosen conveniently and that the SEDRA decay is not dependent on small fluctuations of this frequency can be an advantage. The choice of spinning speed for the distance measurement enables more than one experiment on the same spin pair. If possible, the value of the spinning frequency should be chosen between one and two times the value of the difference between the isotropic chemical shifts. The feasibility of detecting small dipolar couplings depends on the details of the observed molecule as well as on instrumentation. For dipolar strengths of 100 to 50 Hz, an intramolecular distance of 2.2 to 2.5 Å can be measured for a nitrogen spin pair, respectively.

When CSA parameters and dipolar interaction become comparable to the spinning speed, a modified version of t-SEDRA could be employed for the detection of S_0. In this case, ω_0^{eff} in Eq. [15] could also lead to a small imaginary contribution. This in turn leads to terms proportional to Y_0^{23} in the Floquet Hamiltonian, which then assumes the general form of Eq. [13]. Since the Y_0^{23} transforms to $I_{x1}I_{y2} - I_{y1}I_{x2}$ in the effective Hamiltonian, it is evident that properly placed π pulses can eliminate this contribution to zeroth order. Such a sequence is depicted in Fig. 8a. In Fig. 8b the standard t-SEDRA curves are shown for two dipolar interactions, 0.5 and 1.0 kHz, and in Fig. 8c the same curves are shown for the experiment implementing the sequence in Fig. 8a. In practice there is almost no difference between the two sequences for small dipolar interactions, as is the case for the PMP molecule. We preferred the use of the standard t-SEDRA scheme.

Finally, it should be mentioned that the SEDRA cycle and the t-SEDRA cycle can be used in the mixing time of two-dimensional homonuclear correlation spectroscopy experiments. In the first cycle the exchange of polarization is exploited in the RF-driven dipolar recoupling 2D experiments (*3*), whereas in the second cycle, the spin coherence is transferred in order to obtain cross peaks in the 2D spectra (*38*).

APPENDIX A

In the text the MAS Hamiltonian is expressed in terms of $\omega_1^{cs}(t)$, $\omega_2^{cs}(t)$, and $\omega_D(t)$ (*11*). In this appendix their explicit forms are reported.

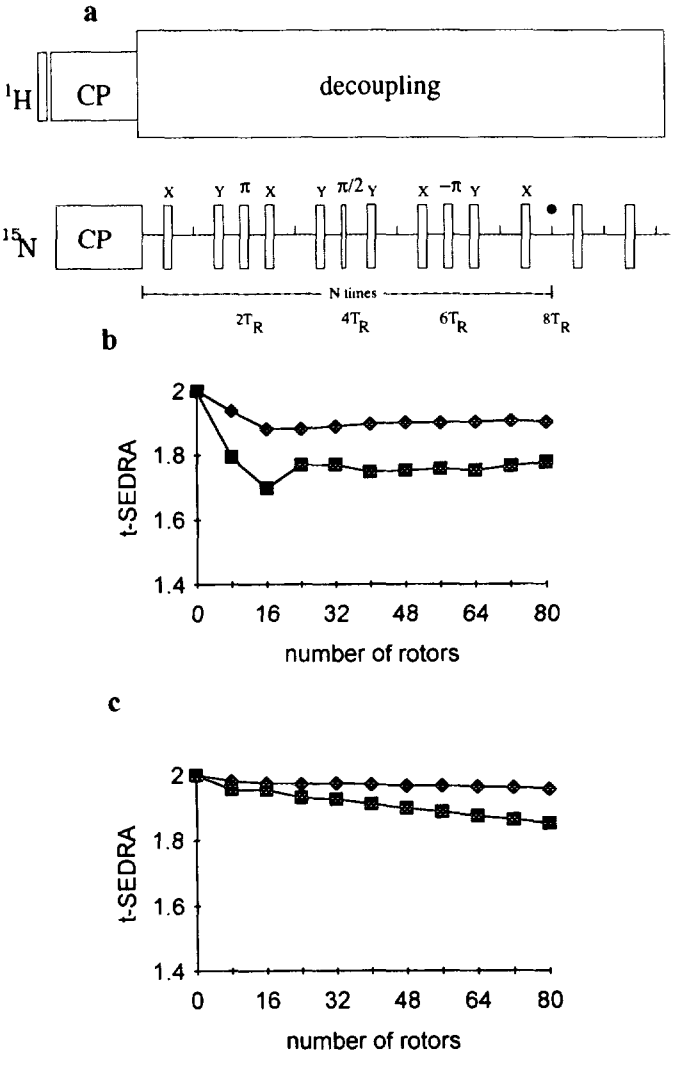

FIG. 8. In (a) the zeroth-order corrected t-SEDRA scheme is shown. t-SEDRA curves using finite pulses illustrating the efficiency of the standard t-SEDRA pulse cycle are calculated. In (b) the standard t-SEDRA cycle was used and in (c) the t-SEDRA with zero-order correction was applied. In both cases, diamonds represent a dipolar strength of 0.5 kHz and squares a dipolar strength of 1.0 kHz. The spinning speed is 2500 Hz and finite pulse intensity is 50 kHz; all other parameters are taken from Table 1.

Chemical Shift

The chemical-shift coefficients of spin-1 or -2 can be written as

$$\omega_i^{cs}(t) = \Delta\omega^i + \omega_1^i\{g_1^i\cos(\omega_R t + \alpha^i + \psi_1^i) + g_2^i\cos(2\omega_R t + 2\alpha^i + \psi_2^i)\}, \quad [A1]$$

where ($i = 1$) for spin-1 and ($i = 2$) for spin-2 and where

$$\Delta\omega^i = \omega_0\sigma_0^i$$

$$\omega_1^i = \omega_0(\sigma_{33}^i - \sigma_0^i)$$

$$\eta^i = \frac{\sigma_{11}^i - \sigma_{22}^i}{\sigma_{33}^i - \sigma_0^i} \quad [A2]$$

are the isotropic chemical shifts, the anisotropic chemical-shift parameter, and the asymmetry parameter, which are all expressed in terms of the principal components (σ_{11}, σ_{22}, σ_{33}) of the chemical-shift-anisotropy tensor. The geometric factors are defined as

$$g_1^i = \frac{\sqrt{2}}{6}\sin\beta^i\sqrt{(\eta^i\cos 2\gamma^i + 3)^2\cos^2\beta^i + \eta^{2i}\sin 2\gamma^i}$$

$$g_2^i = \frac{1}{6}\left(\left[\frac{3}{2}\sin^2\beta^i - \frac{\eta^i}{2}\cos 2\gamma^i(1+\cos^2\beta^i)\right]^2 + \eta^{2i}\cos^2\beta^i\sin^2 2\gamma^i\right)^{1/2}, \quad [A3]$$

and the angles ψ_1 and ψ_2 as

$$\tan\psi_1^i = \eta^i\frac{\sin 2\gamma^i}{(\eta^i\cos 2\gamma^i + 3)\cos\beta^i}$$

$$\tan\psi_2^i = \eta^i\frac{\cos\beta^i\sin 2\gamma^i}{(3/2)\sin^2\beta^i - (\eta^i/2)\times\cos 2\gamma^i(1+\cos^2\beta^i)}. \quad [A4]$$

The angles $(\alpha^i, \beta^i, \gamma^i)$ are the initial Euler angles of the CSA principal-axis systems with respect to the rotor frame.

Dipolar Interaction

The dipolar coupling term in the Hamiltonian of a spin pair can be written as

$$\omega_D(t) = \omega_{12}\{G_1\cos(\omega_R t + \phi_D) + G_2\cos(2\omega_R t + 2\phi_D)\}, \quad [A5]$$

where

$$\omega_{12} = \frac{\mu_0}{4\pi}\frac{\gamma_1\gamma_2}{r_{12}^3}$$

$$G_1 = \frac{\sqrt{2}}{2}\sin\theta_D\cos\theta_D$$

$$G_2 = \frac{1}{4}\sin^2\theta_D, \quad [A6]$$

where θ_D, ϕ_D are the initial polar angles of the vector connecting the spins in the rotor frame, r_{12} is the distance between the spins, and γ_1, γ_2 are the gyromagnetic ratios of the spins.

From the above equations, one can derive the various coefficients appearing in the Floquet Hamiltonians,

$$\begin{aligned}
\omega_0^{14} &= \tfrac{1}{2}(\Delta\omega^1 + \Delta\omega^2) = \tfrac{1}{2}(\omega_1^{cs} + \omega_2^{cs})_0\\
\omega_{\pm1}^{14} &= \tfrac{1}{4}(\omega_I^1 g_1^1 e^{\pm i[\alpha^1+\psi_1^1]} + \omega_I^2 g_1^2 e^{\pm i[\alpha^2+\psi_1^2]})\\
&= (\omega_1^{cs} + \omega_2^{cs})_{\pm1}\\
\omega_{\pm2}^{14} &= \tfrac{1}{4}(\omega_I^1 g_2^1 e^{\pm i[2\alpha^1+\psi_2^1]} + \omega_I^2 g_2^2 e^{\pm i[2\alpha^2+\psi_2^2]})\\
&= (\omega_1^{cs} + \omega_2^{cs})_{\pm2}\\
\omega_0^{23} &= \tfrac{1}{2}(\Delta\omega^2 - \Delta\omega^1) = (\omega_2^{cs} - \omega_1^{cs})_0\\
&= \tfrac{1}{2}\Delta_{12}\\
\omega_{\pm1}^{23} &= \tfrac{1}{4}(\omega_I^2 g_1^2 e^{\pm i[\alpha^2+\psi_1^2]} - \omega_I^1 g_1^1 e^{\pm i[\alpha^1+\psi_1^1]})\\
&= (\omega_2^{cs} - \omega_1^{cs})_{\pm1}\\
\omega_{\pm2}^{23} &= \tfrac{1}{4}(\omega_I^2 g_2^2 e^{\pm i[2\alpha^2+\psi_2^2]} - \omega_I^1 g_2^1 e^{\pm i[2\alpha^1+\psi_2^1]})\\
&= (\omega_2^{cs} - \omega_1^{cs})_{\pm2}\\
\omega_{D\pm1} &= \tfrac{1}{4}\omega_{12}G_1 e^{\pm i\phi_D}\\
\omega_{D\pm2} &= \tfrac{1}{4}\omega_{12}G_2 e^{\pm 2i\phi_D}\\
\Omega_1 &= \tfrac{1}{4}\omega_{12}G_1 \quad [A7]\\
\Omega_2 &= \tfrac{1}{4}\omega_{12}G_2.
\end{aligned}$$

APPENDIX B

Here we derive the expression given in Eq. [10] that relates the eigenvector elements of the Floquet Hamiltonian d_{zn}^{pp} to the Fourier transformation of the function

$$\exp\left\{-\sum_{n=-\infty}^{\infty}\frac{\omega_n^{pp}}{n\omega_R}(e^{in\omega_R t} - 1)\right\}.$$

To derive this relation we assume a general diagonal Hamiltonian of the form

$$\mathcal{H}(t) = 2\sum_p \omega^{pp}(t)I_z^{pp} \quad [B1]$$

that is defined in a manifold of states $|r\rangle$ and that is periodic in time with a basic frequency ω_R:

$$\omega^{pp}(t) = \sum_{n=-\infty}^{\infty}\omega_n^{pp}e^{in\omega_R t}. \quad [B2]$$

The evolution operator corresponding to this Hamiltonian can be evaluated by a simple time integral,

$$\langle p|\mathbf{U}(t)|p\rangle = \langle p|e^{-i\int_0^t\mathcal{H}(\tau)d\tau}|p\rangle, \quad [B3]$$

because the Hamiltonian is self-commuting at all times. Insertion of the expansion for the coefficients ω_n^{pp} results in

$$\langle p|\mathbf{U}(t)|p\rangle = \langle p|\exp\left\{-i\int_0^t 2\sum_{n=-\infty}^{\infty}\omega_n^{pp}e^{in\omega_R\tau}I_z^{pp}\right\}d\tau|p\rangle$$

$$= e^{-i2\omega_0^{pp}t}\langle p|\exp\left\{-2\sum_{n=-\infty}^{\infty}\frac{\omega_n^{pp}}{n\omega_R}\times e^{in\omega_R t}-1]I_z^{pp}\right\}|p\rangle$$

$$= e^{-i2\omega_0^{pp}t}\exp\left\{-\sum_{n=-\infty}^{\infty}\frac{\omega_n^{pp}}{n\omega_R}\times[e^{in\omega_R t}-1]\right\}. \quad [B4]$$

This expression for the element of the evolution operator can be compared with the expression in terms of Floquet theory,

$$\langle p|\mathbf{U}(t)|p\rangle = \sum_{n=-\infty}^{\infty}\langle pn|e^{-i\mathbf{H}_F t}|p0\rangle e^{in\omega_R t}, \quad [B5]$$

with the Floquet Hamiltonian $\mathbf{H}_F$ corresponding to $\mathscr{H}(t)$,

$$\mathbf{H}_F = 2\sum_{n=-\infty}^{\infty}\omega_n^{pp}Z^{pp}. \quad [B6]$$

Inserting the diagonalization matrix $\mathbf{D}_F$ and using $\mathbf{H}_F = \mathbf{D}_F\mathbf{\Lambda}_F\mathbf{D}_F^{-1}$, we get

$$\langle p|\mathbf{U}(t)|p\rangle = \sum_{n,m=-\infty}^{\infty}\langle pn|\mathbf{D}_F|pm\rangle e^{-i(\omega_0^{pp}+m\omega_R)t}\times\langle pm|\mathbf{D}_F^{-1}|p0\rangle e^{in\omega_R t}$$

$$= e^{-2i\omega_0^{pp}t}\sum_{n,m=-\infty}^{\infty}d_{n-m}^{pp}e^{i(n-m)\omega_R t}d_m^{-1\,pp}$$

$$= e^{-2i\omega_0^{pp}t}\sum_{N,m=-\infty}^{\infty}d_N^{pp}e^{iN\omega_R t}d_m^{-1\,pp}$$

$$= e^{-2i\omega_0^{pp}t}\sum_{N=-\infty}^{\infty}d_N^{pp}e^{iN\omega_R t}\left\{\sum_{m=-\infty}^{\infty}d_m^{-1\,pp}\right\}. \quad [B7]$$

In this derivation we used $\langle n|\mathbf{D}_F|m\rangle = d_{n-m}$ and changed the indices of summation n by $N = n - m$. The normalization term $\{\sum_{m=-\infty}^{\infty} d_m^{-1\,pp}\}$ is equal to 1 (*27, 11*); hence we have

$$\langle p|\mathbf{U}(t)|p\rangle = e^{-i\omega_0^{pp}t}\sum_{N=-\infty}^{\infty}d_N^{pp}e^{iN\omega_R t}. \quad [B8]$$

Equalizing Eq. [B7] with Eq. [B4] yields

$$\sum_{N=-\infty}^{\infty}d_N^{pp}e^{iN\omega_R t} = \exp\left\{-\sum_{n=-\infty}^{\infty}\frac{\omega_n^{pp}}{n\omega_R}[e^{in\omega_R t}-1]\right\}. \quad [B9]$$

If we evaluate the complex conjugate of this equation and use the facts that the Hamiltonians are hermitian with $\omega_n^{pp*} = \omega_{-n}^{pp}$ and that the $\mathbf{D}_F$ matrix is unitary with $d_n^* = d_{-n}^{-1}$, the following relation is also valid:

$$\sum_{N=-\infty}^{\infty}d_N^{-1\,pp}e^{iN\omega_R t} = \exp\left\{\sum_{n=-\infty}^{\infty}\frac{\omega_{zn}^{pp}}{n\omega_R}(e^{in\omega_R t}-1)\right\}. \quad [B10]$$

APPENDIX C

In this appendix we show a different route for the calculation of ω_0^{eff}, utilizing the dependence of the d_n coefficients on Bessel functions (*11, 29, 39, 40*). In general this derivation is cumbersome; however, when some approximations can be made, it can become quite easy and useful. In the derivation of Eq. [15], we assumed that the dipolar interaction terms were smaller than the spinning speed, $\omega_n^D \ll \omega_R$. In this case, the dipolar terms in the diagonal blocks of $\mathbf{H}_F^T$ in Eq. [5] can be neglected and the diagonalization matrix $\mathbf{D}_F$ becomes solely dependent on the chemical-shift parameters. Then $\omega_n^{22} = -\omega_n^{33}$, which in turn leads to the connection $d_n = d_n^{22-1} = d_n^{33}$ (*27*) and Eq. [14] becomes

$$\omega_0^{\text{eff}} = -\sum_{k,m=-\infty}^{\infty}d_m d_{-m-k}\Omega_k^x. \quad [C1]$$

If we further simplify the situation by assuming that the chemical-shift anisotropy is small compared to the spinning speed and that only the isotropic chemical-shift values are relevant, then the ω_1^{pp} coefficients in Eq. [11] are equal to

$$\omega_1^{22} = -\omega_1^{33} = \Delta_{12}p_1, \quad [C2]$$

where the p_n coefficients are given by

$$p_{2n-1} = (-1)^{n-1}\frac{2}{(2n-1)\pi}.$$

For this case, the argument of the Bessel functions becomes orientation-independent, which in turn allows us to evaluate the various d_n values for only one arbitrary single crystallite. Using the definitions of Eq. [7] and those of Eq. [A7] of Appendix A and applying

$$J_n = J_n(x) = (-1)^n J_{-n}(x), \quad x = \frac{-2\Delta_{12}}{\pi\omega_R},$$

we obtain the expression for the effective SEDRA frequency

$$\omega_0^{\text{eff}} = 4\Omega_1\cos\phi_d\left\{\frac{1}{2}J_1^2 + \sum_{k=-\infty}^{\infty}J_k J_{2-k}\right\} + 4\Omega_2\cos 2\phi_d\left\{\frac{1}{2}J_2^2 + \sum_{k=-\infty}^{\infty}J_k J_{4-k}\right\} - \frac{J}{2}\sum_{k=-\infty}^{\infty}(-1)^k J_k^2. \quad [C3]$$

In Fig. 2, exact values of ω_0^{eff} for a single crystal are compared

with their approximate value calculated according to this expression. Values for other single crystals gave very similar results. The digital resolution in these simulations was 7.8 Hz/point.

When the above approximations are not valid, because the dipolar strength or the values of the CSA coefficients become comparable to the spinning frequency, the full Floquet Hamiltonian of Eq. [5] must be considered. In such cases, it is advised to use exact numerical calculations for the analysis of the SEDRA experiments.

ACKNOWLEDGMENTS

We thank Dr. J. Elguero, Instituto de Chimica Medica, C.S.I.C., Madrid, for indicating to us the PMP structure problem. We also thank F. Aguilar-Parrilla, Institut für Organische Chemie der Freien, Universität Berlin, for the synthesis of doubly ^{15}N-labeled PMP. O.W. and S.V. thank the Israel–United States Binational Science Foundation, and H.H.L. thanks the Fonds der Chemischen Industrie, Frankfurt, for their financial support.

REFERENCES

1. T. Gullion and S. Vega, *Chem. Phys. Lett.* **194,** 423 (1992).
2. T. Gullion, D. B. Baker, and M. S. Conardi, *J. Magn. Reson.* **89,** 479 (1990).
3. A. E. Bennet, J. H. Ok, S. Vega, and R. G. Griffin, *J. Chem. Phys.* **96,** 8624 (1992).
4. D. K. Sodickson, M. H. Levitt, S. Vega, and R. G. Griffin, *J. Chem. Phys.* **98,** 6742 (1993).
5. E. R. Andrew, S. Clough, L. F. Farnell, T. D. Glendhill, and I. Roberts, *Phys. Lett.* **21,** 505 (1966).
6. D. P. Raleigh, G. S. Harbison, T. G. Neiss, J. E. Roberts, and R. G. Griffin, *Chem. Phys. Lett.* **138,** 285 (1987).
7. D. P. Raleigh, F. Creuzet, M. H. Levitt, and R. G. Griffin, *Isr. J. Chem.* **28,** 263 (1988).
8. M. H. Levitt, D. P. Raleigh, F. Creuzett, and R. G. Griffin, *J. Chem. Phys.* **92**(11), 6347 (1990).
9. T. Nakai and C. A. McDowell, *J. Chem. Phys.* **96,** 3452 (1992).
10. R. Challoner, T. Nakai, and C. A. McDowell, *J. Magn. Reson.* **94,** 433 (1991).
11. A. Schmidt and S. Vega, *J. Chem. Phys.* **96**(4), 2655 (1992).
12. Z. H. Gan and D. M. Grant, *Mol. Phys.* **67,** 1419 (1989).
13. Z. H. Gan and D. M. Grant, *Chem. Phys. Lett.* **168,** 304 (1990).
14. M. M. Maricq and J. S. Waugh, *J. Phys. Chem.* **70,** 3300 (1979).
15. B. H. Meier and W. Earl, *J. Am. Chem. Soc.* **109,** 7937 (1987).
16. R. Tycko and G. Dabbagh, *Chem. Phys. Lett.* **173,** 461 (1990).
17. R. Tycko and G. Dabbagh, *J. Am. Soc.* **113,** 9444 (1991).
18. T. Gullion and J. Schaefer, *Adv. Magn. Reson.* **13,** 57 (1989).
19. T. Gullion and J. Schaefer, *J. Magn. Reson.* **81,** 196 (1989).
20. A. Schmidt, R. A. McKay, and J. Schaefer, *J. Magn. Reson.* **96,** 644 (1992).
21. A. W. Hing, S. Vega, and J. Schaefer, *J. Magn. Reson.* **96,** 205 (1991).
22. R. Tycko, *Phys. Rev. Lett.* **60,** 2734 (1988).
23. R. Tycko, *J. Chem. Phys.* **92,** 5776 (1990).
24. Y. Zur and S. Vega, *J. Chem. Phys.* **79,** 548 (1983).
25. E. M. Krauss and S. Vega, *Phys. Rev. A* **34,** 333 (1986).
26. A. Schmidt and S. Vega, *Isr. J. Chem.* **32,** 215 (1992).
27. O. Weintraub and S. Vega, *J. Magn. Reson. A* **105,** 245.
28. D. B. Zax, G. Goelman, D. Abramovich, and S. Vega, *Adv. Magn. Reson.* **14,** 219 (1990).
29. J. Herzfeld and A. Berger, *J. Chem. Phys.* **73,** 6021 (1980).
30. U. Haeberlen, *Adv. Magn. Reson. Suppl.* **1** (1976).
31. R. R. Ernst, G. Bodenhausen, and A. Wokaun, "Principles of Nuclear Magnetic Resonance in One and Two Dimensions," Clarendon Press, Oxford, 1987.
32. J. Elguero and R. Jacquier, *Bull. Soc. Chim. Fr.*, 2883 (1966).
33. F. Aguilar-Parilla, C. Cativiela, M. Villegas, J. Elguero, C. Foces-Foces, J. I. G. Laureiro, F. H. Cano, H. H. Limbach, J. A. A. Smith, and C. Toiron, *J. Chem. Soc. Perkin. Trans.* **2,** 1737 (1992).
34. Ch. Hoelger, F. Aguilar-Parilla, J. Elguero, and H. H. Limbach, unpublished results.
35. E. N. Masien, J. R. Cannon, A. H. White, and A. C. Willis, *J. Chem. Soc. Perkin. Trans.* **2,** 1298 (1974).
36. V. B. Cheng, *J. Chem. Phys.* **59,** 3992 (1973).
37. F. H. Moore, A. H. White, and A. C. Willis, *J. Chem. Soc. Perkin. Trans.* **2,** 1068 (1975).
38. S. Vega, 34th Experimental NMR Conference, Saint Louis, 1993.
39. G. Goelman, S. Vega, and D. B. Zax, *Phys. Rev. A* **39,** 5725 (1989).
40. D. B. Zax and S. Vega, *Phys. Rev. Lett.* **62,** 1840 (1989).